Supplementary Information: Elucidating the Effect of Mesopores on the Conversion of Green Furans to Aromatics over Hierarchical Ga-MFI, Ga-MFI/MCM-41 Composites, and Ga-SPP.

Guido J.L. de Reijer[†*], Andreas Schaefer[†],
Anders Hellman[‡], Per-Anders Carlsson[†*]

[†]Department of Chemistry and Chemical Engineering,
Chalmers University of Technology,
SE-41296 Gothenburg, Sweden

[‡]Department of Physics,
Chalmers University of Technology,
SE-41296 Gothenburg, Sweden

[*]guidod@chalmers.se; per-anders.carlsson@chalmers.se

Supplementary Information

Table of contents

1. Catalyst synthesis

1.1 Ga-MFI_{meso}

First, tetrapropylammonium hydroxide (TPAOH, 1M in H_2O, ThermoFisher) was diluted with Milli-Q water to form 5 mL 0.2 mol L^{-1} TPAOH solution. Second, 1 g of microporous H-Ga-MFI[1] was added and stirred for 1 h, before transferring the mixture to Teflon-lined stainless-steel autoclave. Dissolution and crystallisation were performed at 170 °C for 24 h, after which the mixture was filtered under vacuum and washed with deionized water. Third, the catalyst was dried overnight using a freeze-drier, after which the dry TPA-Ga-MFI_{meso} was calcined in air for 3 h at 550 °C (2 K min^{-1} ramp), removing the template and producing Ga-MFI_{meso}.

1.2 Ga-MCM-41 and Ga-MFI/MCM-41

Here, a series with different gallium contents was prepared by adjusting the composition of the precursor gel to obtain a final Ga content of 0, 3.1, 8.6, and 11 wt.%, similar to those of the parent material of the first class of catalyst (Ga-MFI_{micro}). First, hexadecyltrimethyl ammonium bromide (CTAB, 99% Sigma-Aldrich) was dissolved in Milli-Q water for 2 h at 70 °C while stirring. Then, a 1.25 mol L^{-1} aqueous NaOH solution (98%, Sigma-Aldrich) was prepared and added, followed by the addition of gallium nitrate hydrate ($Ga(NO_3)_3 \cdot xH_2O$ with x=8 as determined by TGA, 99.9%, Sigma-Aldrich) and dropwise addition of tetraethyl orthosilicate (TEOS, 98%, Sigma-Aldrich). The molar composition

of the synthesis gel was 1 Si: x Ga: 0.12 CTAB: 0.6 NaOH: 127 H_2O, with x=0, x=0.026, x=0.068, and x=0.085 for GO, G3.1, G8.6, and G11, respectively. The synthesis gel was aged for 3 h at RT after which each gel was divided in two equal parts and transferred to two Teflon-lined stainless-steel autoclaves. The sol-gel was crystallised at 100 °C for 3 days, after which one autoclave of each gallium content was removed (Ga-MCM) while the remaining catalysts were further crystallized at 160 °C for 6 days (Ga-MFI/MCM). After crystallisation, the catalyst was filtered under vacuum and washed consecutively with approximately 200 mL deionized water and 100 mL ethanol (95%, Sigma-Aldrich). Afterwards, the catalyst was freeze-dried overnight followed by calcination in air for 5 h at 550 °C (2 K min^{-1} ramp), yielding the Na form of the catalyst. The next step was ion exchange in 1.0 mol L^{-1} NH_4NO_3 for 24 h at RT to produce the NH_4 form of the catalyst (100 mL per gram catalyst). Afterwards, the mixture was filtered, washed with demineralized water, and the cycle was repeated once more for 24 h. After filtration and washing, the catalysts were freeze-dried overnight and then calcined in air for 5 h at 450 °C (2 K min^{-1} ramp), resulting in the protic form of the catalyst.

For catalysts with a higher gallium content, G8.6 and G11, variations were made in the synthesis protocol, resulting in 24 different samples, as described in table S3. Samples 1 (MCM8.6), 2 (MCM11), 3 (MFI/MCM8.6), 4 (MFI/MCM11), 13 (MCM8.6-b), and 15 (MFI/MCM8.6-b) were selected for further structural analysis and catalytic testing. The synthesis of samples 1-4 is described above while for samples 13 and 15, the procedure was the following:

After dissolving CTAB in Milli-Q water for 2 h at 70 °C while stirring, $Ga(NO_3)_3 \cdot 8\,H_2O$ was added and dissolved in 10 minutes. Next, TEOS was added and the solution was hydrolysed for 24 h. Afterwards, the evaporated ethanol and water (formed during hydrolysis and condensation) were replenished by Milli-Q and a 1.43 mol L^{-1} NaOH solution was added dropwise. The synthesis gel was divided into two equal parts; one for crystallisation at 100 °C for 3 days (MCM8.6-b) and one for this step plus crystallisation at 160 °C for 6 days (MFI/MCM8.6-b). Afterwards, the washing, drying, calcination, and ion exchange steps were performed as described above.

1.3 Ga-SPP

First, gallium nitrate hydrate was added to TEOS while stirring after which tetrabutylammonium hydroxide (TBAOH, 40% in H_2O, Sigma-Aldrich) was added dropwise. Next, Milli-Q was added and the solution was hydrolysed for 24 h. The solution was transferred to a Teflon-lined stainless-steel autoclave and crystallised at 120 °C for 5 days. Then, the catalyst was filtered under vacuum and washed with deionized water. This was followed by freeze-drying overnight and a calcination step in air for 10 h at 550 °C (2 K min^{-1} ramp).

2. Flow reactor setup

The catalytic activity of the zeotypes was tested in a fixed-bed reactor consisting of a vertically placed quartz glass tube (⌀=4 mm) surrounded by a metal heating coil for Joule-heating. The temperature of the catalyst was measured by inserting a K-type thermocouple in the powder bed and a second thermocouple was placed in front of the bed to control the temperature of the inlet gas using a PID regulator (Eurotherm, Worthing, UK). The synthesized catalyst powder was pressed into pellets (10 tonnes) and subsequently ground to a particle size of 355 µm to 450 µm to avoid a pressure drop. Roughly 75 mg (70 mg to 100 mg) of catalyst powder was loaded and held in place by two plugs of silanized quartz wool (Sigma-Aldrich). The feed gases Ar, O_2, and NH_3 were introduced via mass flow controllers (MFCs, Bronkhorst Hi-Tech, Low-Δ-P-flow) and Ar was used as carrier gas through a gas saturator containing liquid 2,5-dimethylfuran (Apollo scientific, 99% or Sigma-Aldrich, 99%) at room temperature; the total flow was kept constant at 300 mL/min, resulting in a 2,5-dmf concentration of ca. 720 ppm. The effluent gas mixture was analysed online with a Fourier-transform infrared (FTIR) spectroscope gas analyser (MKS MultiGas 2030). Products were quantified with the MKS software suite MG2000 v.10.2 and FTIR-library v.R3 by FTIR according to a method described in previous work.[2;3] Details of the IR-bands are shown in table S1. The gas mixture is scanned each second and IR spectra are recorded every 2 or 15 s between 4000 cm^{-1} to 600 cm^{-1} with a resolution of 0.5 cm^{-1}. Before the conversion experiment, a background spectrum was recorded in Ar. Stainless-steel tubing before and after the reactor and the IR cell were kept at a constant temperature of 191 °C to prevent condensation of reagents and products.

3. Procedures for catalytic performance tests and NH_3-TPD

Before each conversion experiment, the catalyst was pretreated in 20 % O_2 in Ar for 30 min at 100 °C followed by 1 h at 500 °C (10 °C/min) to remove adsorbed species such as water. Following this, an NH_3-TPD was performed to determine the acid site density of the fresh catalyst. First, the catalyst was saturated at 100 °C by flowing 300 ppm NH_3 for 90 min followed by purging in Ar for 90 min to desorb the loosely bound physisorbed ammonia. Second, the temperature was increased to 600 °C (10 °C/min), and the desorbed ammonia was detected and quantified with FTIR, assuming that one acid site adsorbs one ammonia molecule. The TPD profile was fitted by symmetric Gaussian functions after a linear background had been subtracted. The catalyst dwelled at 600 °C for 20 min to ensure complete ammonia desorption after which the temperature was reduced to 500 °C and 720 ppm of 2,5-dmf was introduced and flowed for 3 h. Directly after the reaction, another NH_3-TPD was performed according to the method described above to determine the number and type of acid sites that are available on the coked catalyst.This was followed by the oxidative regeneration of the catalyst in 20 % O_2 for 90 min at 600 °C (5 °C/min) or a

temperature-programmed oxidation by cooling down to 600 °C before ramping up to 600 °C (10 °C/min). This was followed by a third NH_3-TPD.

The zeotypes G6.0$_{meso}$, G6.7$_{meso}$, G8.6$_{meso}$, and G11$_{meso}$, were exposed to four additional cycles of 3 h 2,5-dmf conversion at 500 °C, separated by oxidative regeneration steps. After the fifth cycle, a fourth NH_3-TPD was performed.

Table S1: An overview of the detected species and the primary spectral ranges for their quantification with an FTIR spectrometer. For analysis so-called primary analysis regions, which are narrower than the primary spectral regions, are selected according to a previously described analysis method with adaptions.[2;3;4]

Molecule	Formula	IR band /cm^{-1}
BTX		
Benzene	C_6H_6	606.51 – 726.80
Toluene	C_7H_8	680.58 – 776.94
para-xylene	C_8H_{10}	735.32 – 867.92
Furans		
2,5-dimethylfuran	C_6H_8O	1168.43 – 1282.69
2,4-dimethylfuran	C_6H_8O	1074.17 – 1174.70
2-methylfuran	C_5H_6O	1117.57 – 1176.87
Other rings		
2-MCPO	C_6H_8O	1668.88 – 1809.90
3-MCPO	C_6H_8O	1701.42 – 1811.83
Indene	C_9H_8	2811.26 – 3176.23
2-methylnaphthalene	$C_{11}H_{10}$	785.38 – 831.18
Naphthalene	$C_{10}H_8$	758.62 – 807.32
Olefins		
Ethene	C_2H_4	900.12 – 1000.16
Propene	C_3H_6	900.61 – 1019.69
1,3-butadiene	C_4H_6	822.26 – 977.02
C1		
Methane	CH_4	3000.25 – 3176.23
Carbon monoxide	CO	2146.16 – 2159.90
Carbon dioxide	CO_2	2223.57 – 2280.94
Formaldehyde	CH_2O	2698.93 – 2822.36
Other		
Water	H_2O	1416.97 – 1502.31
Ammonia	NH_3	903.98 – 977.27

4. Procedure for pyridine DRIFTS

Pyridine adsorption was studied by DRIFTS using a Bruker VERTEX 70 equipped with a mercury cadmium telluride detector (bandwidth 600 to 12000 cm^{-1}) cooled with liquid nitrogen, a Praying Mantis™ Diffuse Reflectance accessory (Thermo Scientific™), and a stainless-steel high-temperature reaction chamber (Harrick Scientific Products, Inc.) with CaF_2 windows. The setup was modified in-house to allow for probing with liquid pyridine by using a gas saturator and argon as a carrier gas, as shown in other work (figure S1 [1]). First, the catalyst bed was partially filled with IR-inactive KBr to limit sample loss, after which roughly 20 mg of the catalyst was added on top (particle size of 40 µm to 80 µm). Then the catalyst was pretreated in 15% O_2 in Ar for 60 min at 300 °C (15 °C/min), maintaining a total flow of 100 mL/min. After pretreatment, background spectra were recorded at 150 and 300 °C in Ar. This was followed by saturation with pyridine at 300 °C by flowing 1 mL/min Ar through the gas saturator for 35 min. Next, physisorbed pyridine was removed by purging in Ar for 45 min, after which a background subtracted spectrum was recorded between 4000 cm^{-1} to 800 cm^{-1} composed of 64 scans (resolution of 1 cm^{-1}). Afterward, the temperature was lowered to 150 °C and the pyridine adsorption/desorption cycle was performed again. The temperature was monitored via a thermocouple located in the centre of the catalyst bed.

The acid sites were quantified by integrating the peaks corresponding to the vibrations of pyridine bonded to Brønsted and Lewis acid sites. First, the background was optimized by fitting an Akima spline function over the region 1650 cm^{-1} to 1400 cm^{-1}. Second, the peak around 1545 cm^{-1} was integrated for BAS (peak center ± 25 cm^{-1}) and the peak around 1455 cm^{-1} for LAS (peak center ± 15 cm^{-1}), assuring no overlap with neighbouring peaks. The integrated areas were corrected for the difference in molar attenuation coefficients, or molar extinction coefficients ϵ (ϵ_{BAS}=1.67 cm µmol^{-1}, ϵ_{LAS}=2.22 cm µmol^{-1}) [5].

5. Conversion and selectivity

Principally molar flows should be used to calculate reactant conversion and reaction selectivity for continuous processes. Here, however, diluted conditions is used and the total molar flow is to a good approximation constant and the ideal gas law applies. Thus, one can base both conversion and selectivity on concentrations. The furan conversion X can be calculated as:

$$X = 1 - \frac{C_{\text{2,5-dmf}}}{C_{\text{2,5-dmf, 0}}} \approx 1 - \frac{C_{\text{2,5-dmf}}}{\sum \frac{n_i}{6} \cdot C_{\text{product,i}} + C_{\text{2,5-dmf}}} \tag{1}$$

where $C_{\text{2,5-dmf, 0}}$ is the inlet concentration of 2,5-dmf, $C_{\text{2,5-dmf}}$ is the measured outlet concentration of 2,5-dmf, and $C_{\text{product,i}}$ is the measured concentration of product i. The approximation is valid for 2,5-dmf conversion to gas products. Here, the product concentrations C are normalized to account for the reaction stoichiometry by multiplication with

their number of carbon atoms n_i, followed by division by the number of carbon atoms in the reactant 2,5-dmf (6 carbon atoms). Similarly, the selectivity of each species can be calculated as follows:

$$S = \frac{n_i \cdot C_{\text{product,i}}}{6 \sum \frac{n_i}{6} \cdot C_{\text{product,i}}} \tag{2}$$

6. Elemental composition

Table S2: Elemental compositions of the synthesised catalysts measured by XRF, normalised to a total sum of 100 wt.%.

Sample	Si/Ga_{micro} [1]	Si/Ga_{meso}	Ga	Si	O[a]	Na	K	Ca	Cu	Br	H_2O[b]
					wt.%						
$G1.2_{meso}$	95	81	1.4	45.3	53.0	0	0.2	0	0	0	1.0
$G3.1_{meso}$	34	27	3.9	43.1	52.1	0	0.6	0	0	0	1.7
$G6.0_{meso}$	17	22	4.8	42.3	51.9	0.2	0.5	0	0	0	2.0
$G6.7_{meso}$	15	19	5.3	40.9	52.7	0	0.6	0.01	0	0	3.9
$G8.6_{meso}$	11	15	6.8	39.8	51.5	0	1.4	0.02	0	0	4.7
$G11_{meso}$	8	11	8.5	37.4	51.6	0.4	1.3	0.01	0	0	6.4
SPP1.2	N.A.	93	1.2	44.7	52.8	0	1.2	0	0	0.003	1.3
SPP2.4	N.A.	45	2.4	43.5	52.2	0	1.4	0	0.01	0.4	1.7
SPP3.6	N.A.	29	3.6	42.9	52.0	0	1.3	0	0.01	0	1.8

[a] Derived by assuming metals to be present as oxides; [b] Determined by TGA.

7. Structural characterisation

To explore the synthetic feasibility of Ga-MFI/MCM-41 composites with a high Ga-content, additional materials were prepared that address the influence of the base concentration, the alkali source (NaOH vs KOH), and the ageing conditions. An overview of the precursor gel compositions is shown in table S3 and the XRD diffractograms are shown in figure S1.

As the hydrolysis and subsequential condensation of TEOS into a cross-linked prezeolitic silica network can be catalyzed both by base and acid, NaOH can be added directly to H_2O, TEOS, and $Ga(NO_3)_3 \cdot 8\,H_2O$, or after the hydrolysis step initialized by the acidic Ga precursor. Base ageing conditions resulted in the samples 1-4 (figure 1), a procedure successful for lower Ga contents. Ageing under acidic conditions resulted in MCM8.6 (#5) with peaks associated to the MCM-41 structure (green bars), while MCM-11 (#5) displays lower SNR and less well-defined peaks. The second crystallisation step (6d at 160 °C) resulted in sharper peaks but no transformation into MFI (#7 & #8). Increasing the acidic ageing duration from 3h to 24h, increased the SNR for MCM11 (#10), demonstrating the importance of ageing to facilitate crystallization. On the contrary, MCM8.6 (#9) has a low SNR, possibly

due to the slightly lower pH and higher gallium-to-base ratio; Ga/OH^-=0.17 for sample #9 compared to 0.16 for sample #5. The second high-temperature step to produce samples #11 and #12 decreases the crystallinity of MCM11, while MCM8 appears unchanged. This suggests that the combination of the relatively higher base content (OH^-/Si=0.43) of MFI/MCM11 (#12) and the high temperature promotes the dissolution of the MCM11 framework, while not favouring recrystallisation into MCM-41 or MFI structures.

To further analyse the role of the base concentration, the amount of base was increased incrementally for samples #13 and #14 (MCM8.6) to OH^-/Si=0.82 and 1.21, respectively. The peaks of sample #13, also displayed in figure 1 as MCM-8.6-b, are sharp and positioned at 2.6, 4.4, 5.0, and 6.7°; a slight deviation to what was observed for Al-MCM-41 in other work[6]. No peaks were identified for sample #14, suggesting that the pH was too high to synthesize MCM. However, when only a small quantity of material is produced and measured, a much smaller volume is probed by X-rays and thus the intensity of the diffracted X-rays and SNR will be much lower, rendering peak identification challenging, as was the case for samples 1, 2, 14, and 16. For MFI/MCM8.6 (#15), also displayed in figure 1 as MFI/MCM-8.6-b, sharp peaks are resolved at 2.2, 3.7, 4.2, and 5.6°. The peaks have shifted to lower angles compared to its MCM analog, with differences of 0.4 to 1.1°, indicating an increase in d-spacing and thus an increase in the average mesopore size. It is proposed that this results from the partial dissolution of the inner wall of the mesopores of MCM8.6, which was formed in the first low-temperature crystallisation step. Consecutive recrystallisation of the dissolved species into MFI was not observed, possibly since the pH was still too low.

However, a further increase in base concentration to Ga/OH^-=0.4 used for samples 17-20, did not result in the synthesis of more than a few milligrammes of material. Additionally, when these high base concentrations were used and the base was added at the start of the ageing step, basic ageing, no precursor gel was formed (sample 21-24). Instead, for MFI/MCM11 (#22), a gallium analog of the tectosilicate natrolite[7] (red bars) was identified as the main crystalline phase. When using a different alkali source at high concentrations, KOH instead of NaOH, an unidentified crystal phase is formed for both MFI/MCM8.6 and MFI/MCM11 (#23 & #24). In other work,[8] a promoting effect of KOH was observed on the transformation of dissolved nutrients into MFI, owing to the enhanced dissolution of silica from MCM-41 and amorphous silica by K^+,[9;10] ultimately enhancing electrostatic interactions between silica and the head group of CTA^+.[11] Here, this effect was not observed due to the high pH, preventing the initial formation of an MCM-41 structure.

The 24 unsuccessful attempts at the one-pot synthesis of Ga-MFI/MCM-41 composites with high gallium contents demonstrate the difficulty of the synthesis, the delicate role of the acidity and precursor composition, as well as the potential disruptive role of the large gallium ion and its acidic precursor. While the initial base concentration needs to be sufficiently high to promote Ga-MCM-41 formation at low temperatures, an excessively high pH will prevent the latter's formation at all. Simultaneously, a high pH is needed to induce partial dissolution and subsequent transformation into MFI at high temperatures,

although complete dissolution needs to be prevented too.

Table S3: Overview of the different synthesis conditions used to synthesize high gallium-content MCM-41 and MFI/MCM-41 materials.

#	Structure[a]	Ga/Si	OH^-/Si	Ga/OH^-	Ageing cond.[b]	Ageing dur.[c]	pH[d]
1[e]	MCM8.6	0.07	0.62	0.11	Basic	3	12
2[e]	MCM11	0.09	0.70	0.12	Basic	3	12
3[e]	MFI/MCM8.6	0.07	0.66	0.11	Basic	3	12
4[e]	MFI/MCM11	0.09	0.65	0.13	Basic	3	12
5	MCM8.6	0.07	0.43	0.16	Basic	3	12
6	MCM11	0.08	0.43	0.19	Acidic	3	12
7	MFI/MCM8.6	0.07	0.43	0.16	Acidic	3	12
8	MFI/MCM11	0.08	0.43	0.19	Acidic	3	12
9	MCM8.6	0.07	0.41	0.17	Acidic	24	11
10	MCM11	0.08	0.43	0.19	Acidic	24	11
11	MFI/MCM8.6	0.07	0.41	0.17	Acidic	24	11
12	MFI/MCM11	0.08	0.43	0.19	Acidic	24	11
13[f]	MCM8.6	0.07	0.82	0.09	Acidic	24	13
14	MCM11	0.07	1.21	0.06	Acidic	24	13
15[f]	MFI/MCM8.6	0.07	0.82	0.09	Acidic	24	13
16	MFI/MCM11	0.07	1.21	0.06	Acidic	24	13
17	MCM8.6	0.07	1.70	0.04	Acidic	24	14
18	MCM11	0.09	2.00	0.04	Acidic	24	14
19	MFI/MCM8.6	0.07	1.70	0.04	Acidic	24	14
20	MFI/MCM11	0.09	2.00	0.04	Acidic	24	14
21	MFI/MCM8.6	0.07	1.72	0.04	Basic	24	14
22	MFI/MCM11	0.08	2.12	0.04	Basic	24	14
23[g]	MFI/MCM8.6-KOH	0.07	1.68	0.04	Basic	24	14
24[g]	MFI/MCM11-KOH	0.08	2.00	0.04	Basic	24	14

[a] MCM structures were crystallised for 3 d at 100 °C, MFI/MCM for 3 d at 100 °C + 6 d at 160 °C. The number denotes the aimed gallium content in wt.%; [b] Hydrolysis and condensation of TEOS occurs under both basic or acidic conditions. *Basic* indicates that TEOS and Ga are added to NaOH or KOH solution. *Acidic* means TEOS was added to acidic gallium precursor solution, and the base was added after an initial ageing step; [c] Hydrolysis duration in hours; [d] Approximate pH of precursor solution at the end of ageing, determined with dosatest pH indicator (VWR); [e] Materials shown in figure 1 as MCM8.6, MCM11, MFI/MCM8.6, and MFI/MCM11 ; [f] Materials shown in figure 1 as MCM8.6-b and MFI/MCM8.6-b.; [g] KOH used as base instead of NaOH;

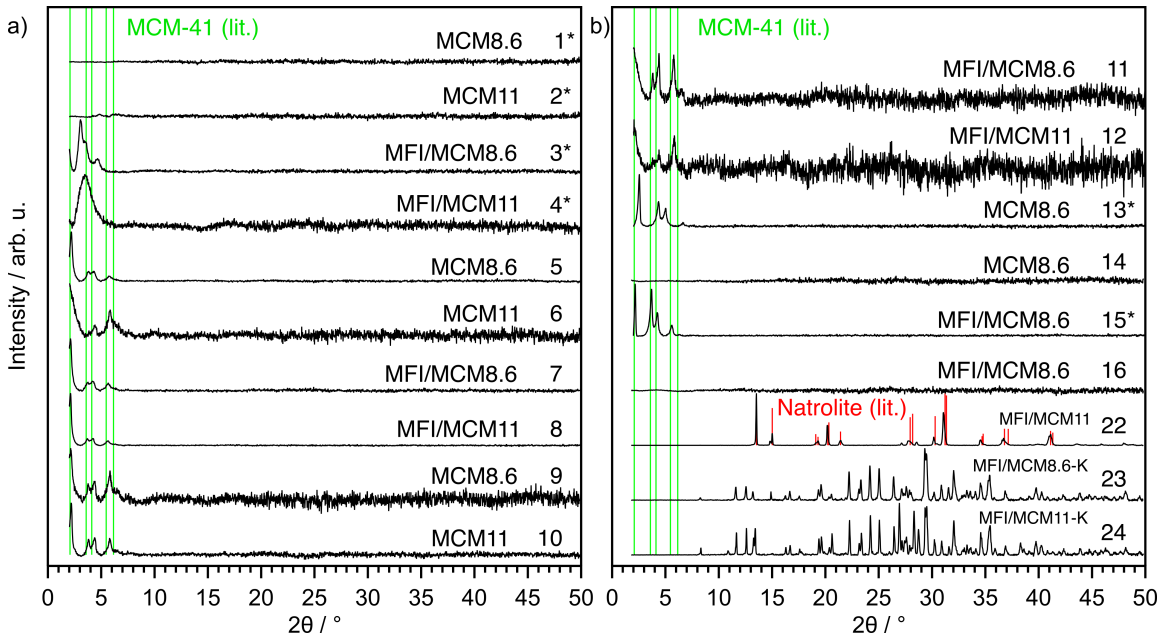

Figure S1: XRD diffractograms of Ga-MCM and Ga-MFI/MCM-41 with high gallium loadings synthesized with varying precursor gel composition, pH, and ageing conditions. The synthesis conditions of each sample are shown in table S3. Samples 1, 2, 3, 4, 13, and 15 were used for further structural analysis and catalytic testing, as described in the main text. Reference structures are mesoporous MCM-41[6] (green bars) and natrolite[7] (red bars). All diffractograms are normalized to their highest intensity except for samples 1, 2, 14, and 16, since no peaks were distinguished.

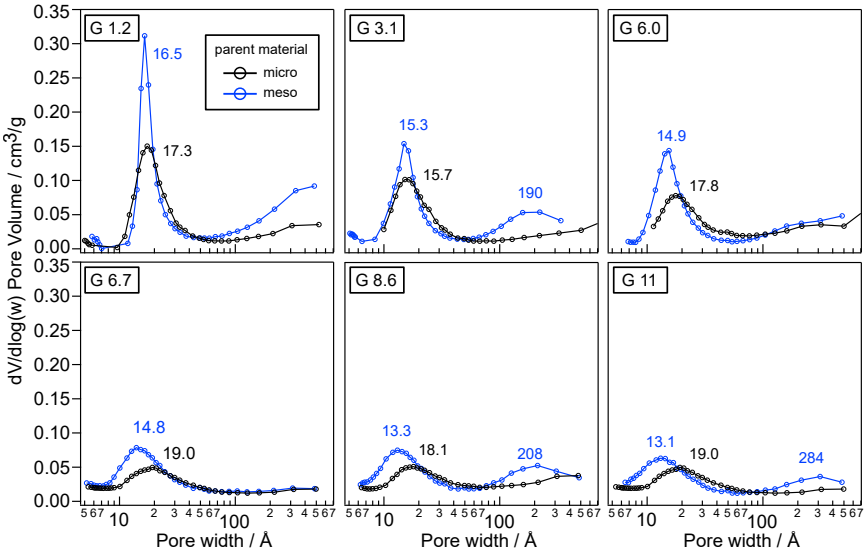

Figure S2: Pore size distributions estimated from the nitrogen adsorption isotherm at 77 K using the BJH model with Harkins-Jura thickness model for the Ga-MFI$_{\text{micro}}$ (black) and Ga-MFI$_{\text{meso}}$ (blue) with different Ga content as indicated on the panels.

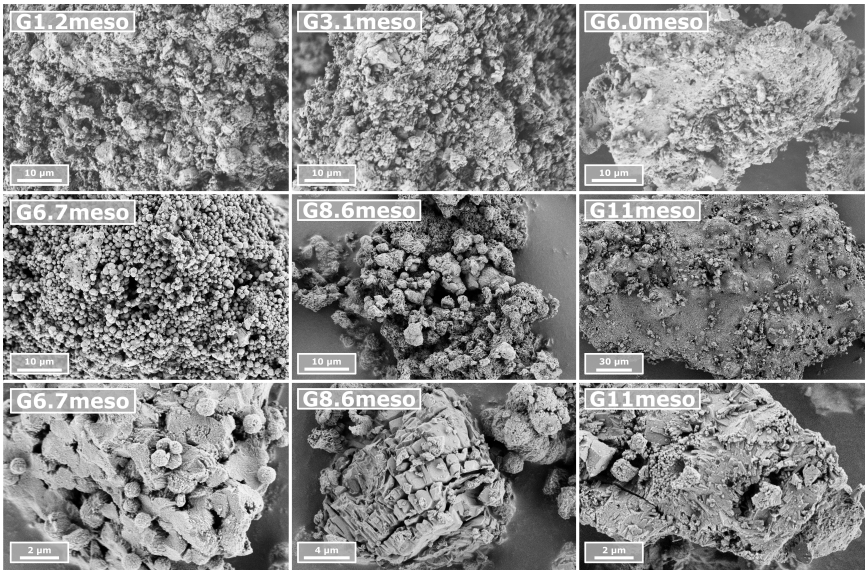

Figure S3: SEM images of the calcined mesoporous Ga-MFI zeotypes, including a close-up of the high gallium content zeotypes in the bottom row. Images are recorded at an accelerating voltage of 1 kV (G1.2$_{\text{meso}}$, G3.1$_{\text{meso}}$, G6.0$_{\text{meso}}$) or 1.5 kV (G6.7$_{\text{meso}}$, G8.6$_{\text{meso}}$, G11$_{\text{meso}}$) using secondary electrons (SE2 detector).

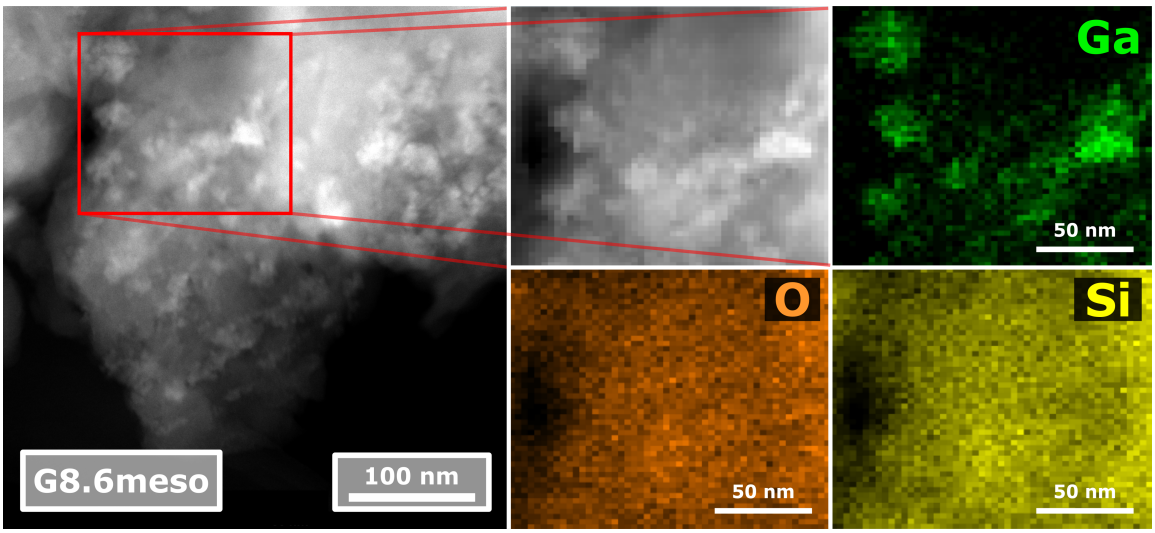

Figure S4: HAADF-STEM image of G8.6$_{\text{meso}}$ as well as an EDX map of the ROI indicated by the red box, displaying the dispersion of gallium, oxygen, and silicon. Pixel size of 3 nm.

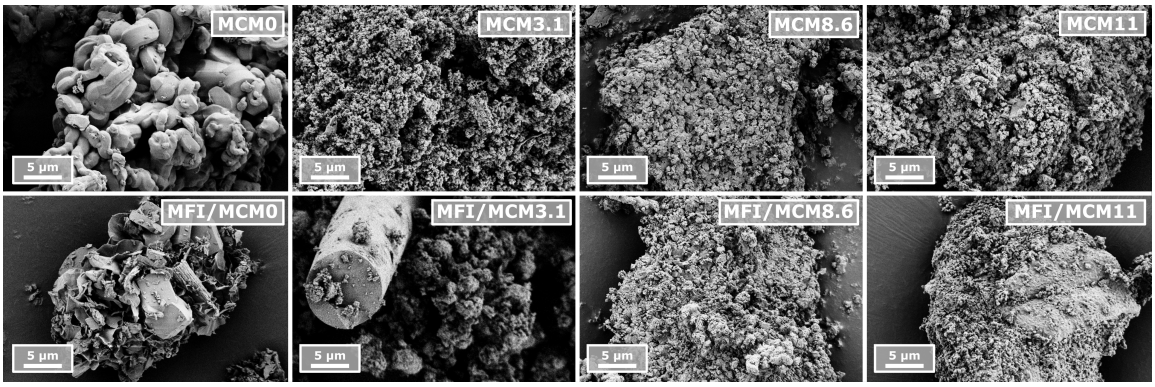

Figure S5: SEM images of H-Ga-MCM-41 (synthesis 1, top row) and H-Ga-MFI/MCM-41 (synthesis 1, bottom row), recorded at an accelerating voltage of 1.5 kV. Samples were sputter-coated with gold (2 nm) to prevent charging effects.

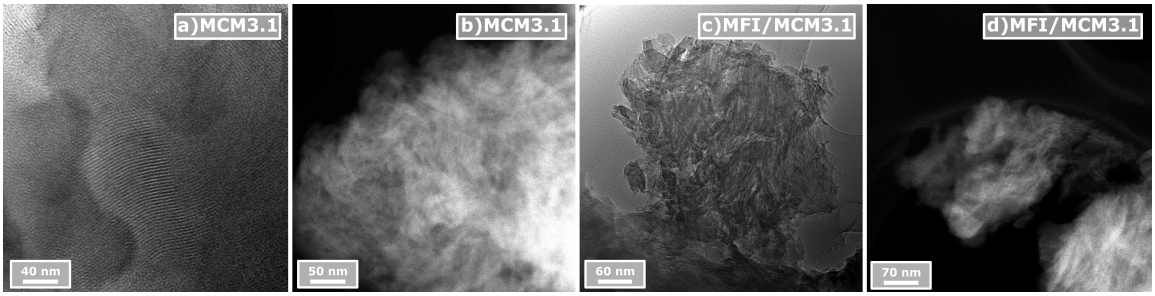

Figure S6: TEM images of H-Ga-MCM3.1 (a) H-Ga-MFI/MCM3.1 (c) and HAADF-STEM images and of H-Ga-MCM3.1 (b) H-Ga-MFI/MCM3.1 (d). Images were recorded with an accelerating voltage of 300 kV.

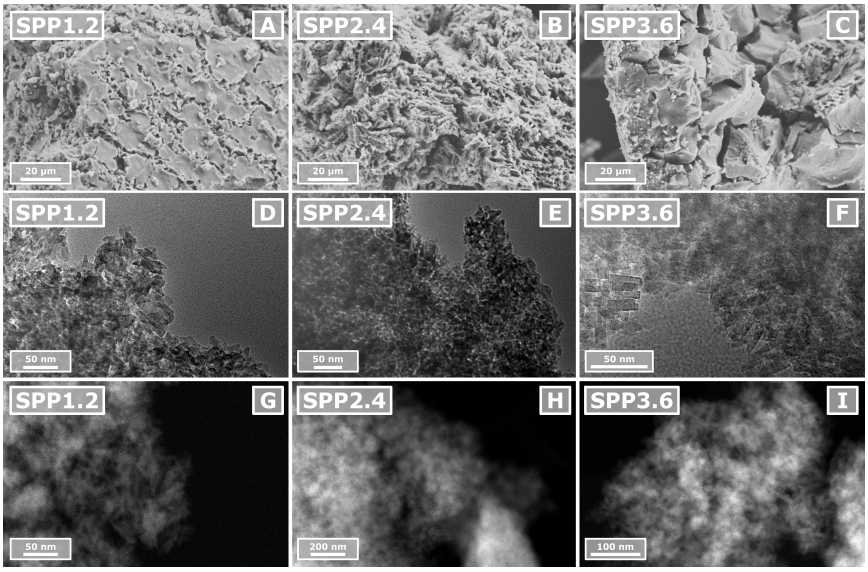

Figure S7: Electron images of Ga-SPP catalysts including SEM images (A, B, C), TEM images (D, E, F) and HAADF-STEM images (G, H, I). Accelerating voltages of 10 kV (SEM) or 300 kV (TEM/HAADF-STEM) were used.

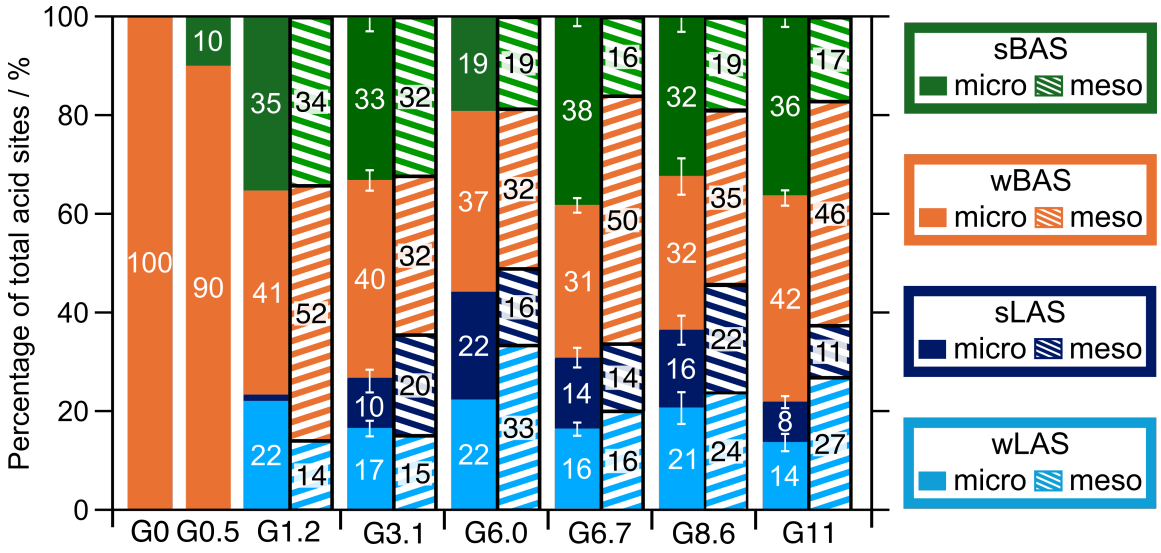

Figure S8: SI figure: Distribution of the acid sites of Ga-MFI$_{micro}$ [1] (filled) and Ga-MFI$_{meso}$ (patterned), given as a percentage. Sites are classified into strong and weak Brønsted acid sites (sBAS and wBAS) as well as strong and weak Lewis acid sites (sLAS and wLAS). Several microporous Ga-MFI$_{micro}$ were measured twice and the error bars indicate the deviations from the average values; determined by pyridine adsorption DRIFTS.

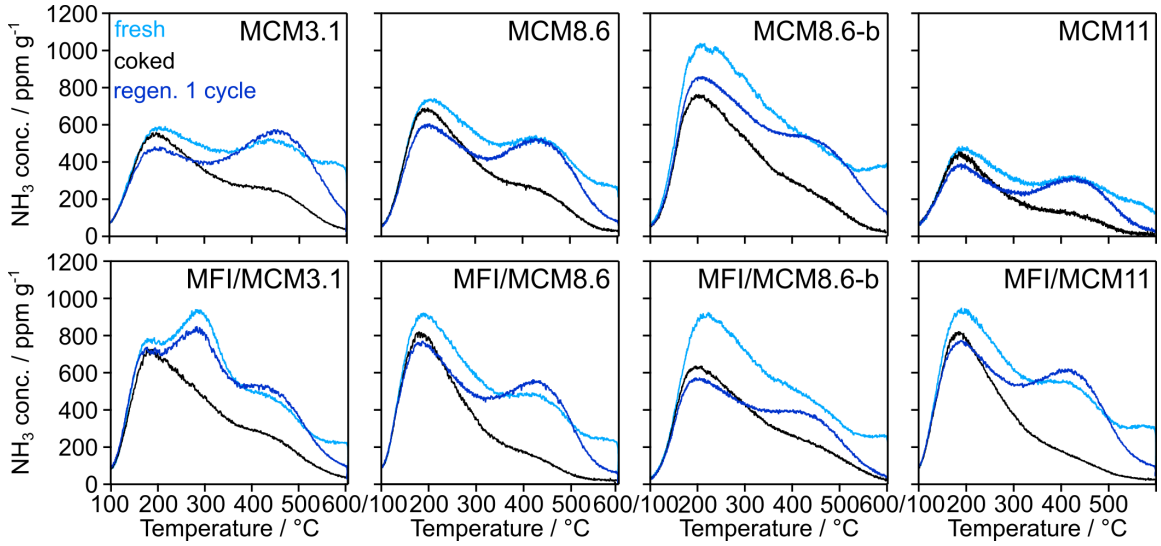

Figure S9: NH_3-TPD profiles of Ga-MCM-41 and Ga-MFI/MCM-41 catalysts before the reaction (fresh, light blue), directly after the reaction (coked, black), as well as after an oxidative regeneration (regen., dark blue)

Table S4: Quantification of the NH_3-TPD profiles of fresh microporous parent zeotype Ga-MFI_{micro}, fresh mesoporous zeotypes Ga-MFI_{meso}, coked, regenerated after 1 cycle, and regenerated after 5 cycles. The percentages of acid sites remaining with respect to the fresh micro- or mesoporous zeotypes are shown.

Sample	status	Acid site density $mmol\,g^{-1}$	% acid sites w.r.t. fresh
G1.2m	$fresh_{micro}$	0.119	100
	$fresh_{meso}$	0.052	44*
	$coked_{meso}$	0.002	4
G3.1m	$fresh_{micro}$	0.268	100
	$fresh_{meso}$	0.124	46*
	$coked_{meso}$	0.022	18
G6.0m	$fresh_{micro}$	0.256	100
	$fresh_{meso}$	0.140	55*
	$coked_{meso}$	0.026	18
	regen. $1c_{meso}$	0.141	101
	regen. $5c_{meso}$	0.170	121
G6.7m	$fresh_{micro}$	0.423	100
	$fresh_{meso}$	0.249	59*
	$coked_{meso}$	0.038	15
	regen. $1c_{meso}$	0.229	92
	regen. $5c_{meso}$	0.206	83
G8.6m	$fresh_{micro}$	0.433	100
	$fresh_{meso}$	0.212	49*
	$coked_{meso}$	0.023	11
	regen. $1c_{meso}$	0.166	78
	regen. $5c_{meso}$	0.152	72
G11m	$fresh_{micro}$	0.612	100
	$fresh_{meso}$	0.354	58*
	$coked_{meso}$	0.094	26
	regen. $1c_{meso}$	0.321	91
	regen. $5c_{meso}$	0.281	79

*w.r.t. fresh microporous parent zeotype

Table S5: Quantification of the NH_3-TPD profiles of fresh Ga-MCM-41 and Ga-MFI/MCM-41, coked, and regenerated after 1 cycle. The percentages of acid sites remaining with respect to the fresh catalyst are shown.

Sample	status	Acid site density $\mathrm{mmol\,g^{-1}}$	% acid sites w.r.t. fresh
MCM3.1	fresh	0.265	100
	coked	0.151	57
	regen. 1c	0.227	86
MCM8.6	fresh	0.280	100
	coked	0.166	59
	regen. 1c	0.230	82
MCM8.6b	fresh	0.316	100
	coked	0.205	65
	regen. 1c	0.281	89
MCM11	fresh	0.161	100
	coked	0.082	51
	regen. 1c	0.125	77
MFI/MCM3.1	fresh	0.309	100
	coked	0.177	57
	regen. 1c	0.278	90
MFI/MCM8.6	fresh	0.285	100
	coked	0.146	51
	regen. 1c	0.248	87
MFI/MCM8.6b	fresh	0.327	100
	coked	0.183	56
	regen. 1c	0.207	63
MFI/MCM11	fresh	0.313	100
	coked	0.154	49
	regen. 1c	0.263	84

8. Catalytic performance tests and long-term stability

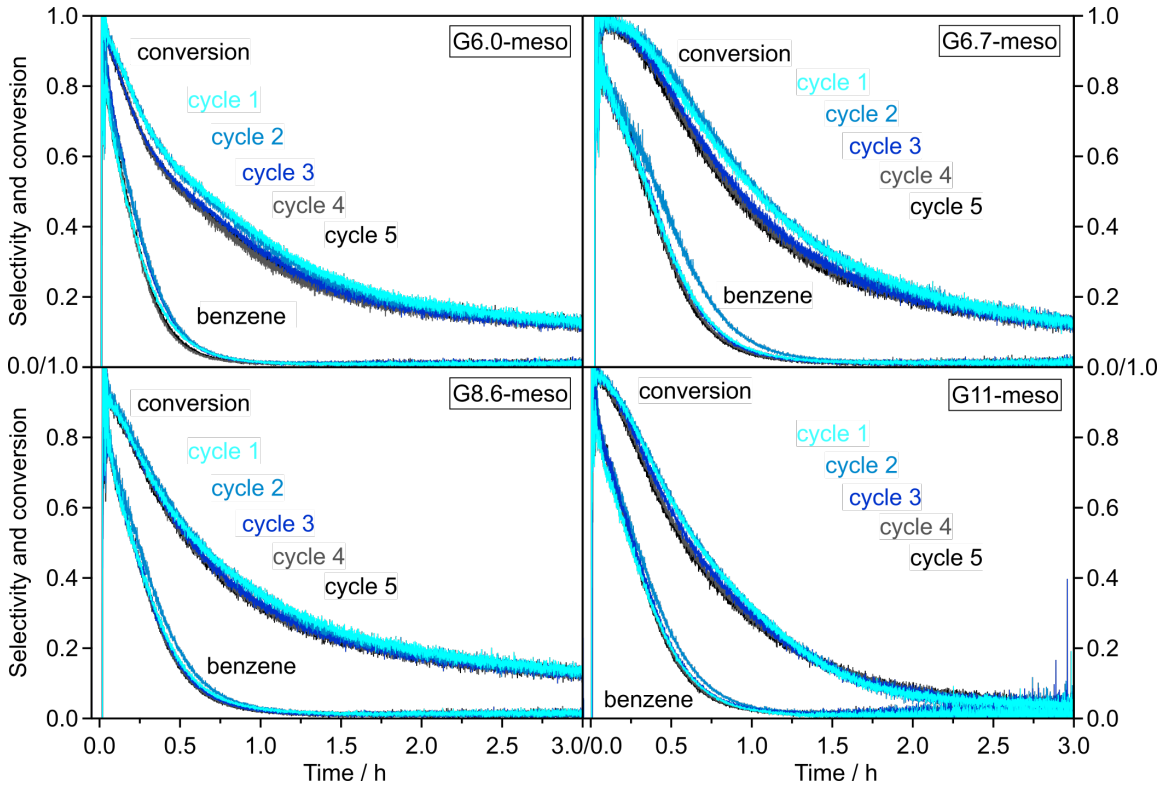

Figure S10: Conversion of 2,5-dmf and benzene selectivity over four mesoporous Ga-MFI zeotypes for the course of five cycles of 3 h conversion at 500 °C separated by 1 h calcination in 20 % O_2 at 600 °C.

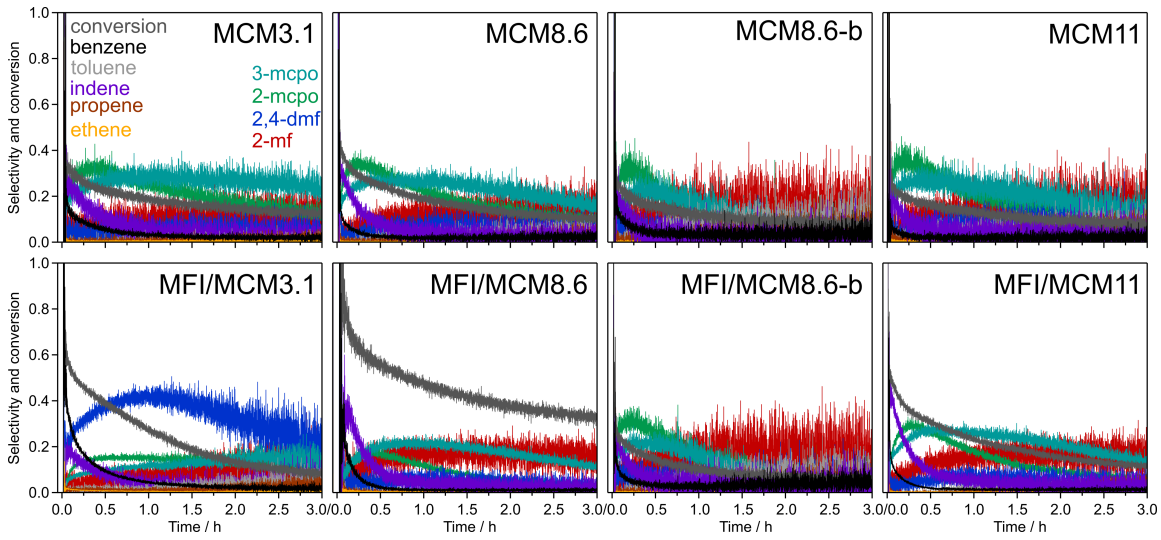

Figure S11: Conversion of 2,5-dmf and selectivities of the main products over Ga-MCM-41 and Ga-MFI/MCM-41 with 3 h TOS at 500 °C. Concentrations were determined every 2 s.

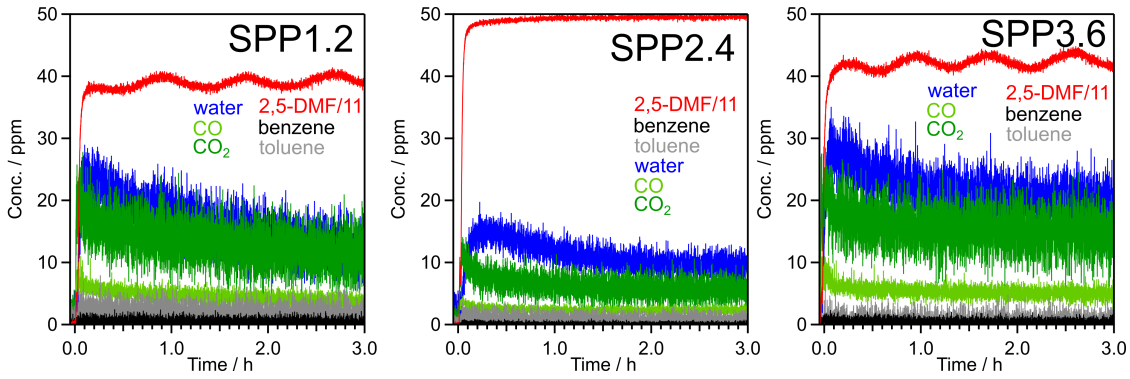

Figure S12: Concentrations of the main products detected over Ga-SPP catalysts during 3 h 2,5-dmf conversion at 500 °C. Concentrations were determined every 2 s. The concentration of the reactant 2,5-dmf (red) was divided by 11 to fit on the same axis.

References

(1) Guido J.L. de Reijer, Andreas Schaefer, Anders Hellman, and Per Anders Carlsson. Catalytic Conversion of Furans to Aromatics over Ga-MFI Zeotypes with Varying Gallium Content. *Industrial and Engineering Chemistry Research*, 64(4):2025–2035, 2025.

(2) Christopher Sauer, Guido J. L. de Reijer, Andreas Schaefer, and Per-Anders Carlsson. Isomorphous Substitution of Gallium into MFI-Framework Zeolite Increases 2,5-Dimethylfuran to Aromatics Selectivity and Suppresses Catalyst Deactivation. *Topics in Catalysis*, 66(17-18):1329–1340, 2023.

(3) Christopher Sauer, Anders Lorén, Andreas Schaefer, and Per-Anders Carlsson. On-Line Composition Analysis of Complex Hydrocarbon Streams by Time-Resolved Fourier Transform Infrared Spectroscopy and Ion-Molecule Reaction Mass Spectrometry. *Analytical Chemistry*, 93(39):13187–13195, 2021.

(4) Christopher Sauer, Guido J. L. de Reijer, Barbara Wilfinger, Anders Hellman, and Per-Anders Carlsson. Continuous isomerisation of 2,5-dimethylfuran to 2,4-dimethylfuran over Ga-silicate. *Chemistry – A European Journal*, 30(20), 2024.

(5) C. A. Emeis. Determination of integrated molar extinction coefficients for infrared absorption bands of pyridine adsorbed on solid acid catalysts. *Journal of Catalysis*, 141(2):347–354, 6 1993.

(6) Maria J.F. Costa, Thiago Chellappa, Antonio S. Araujo, Viviane M. Fonseca, Valter J. Fernandes, Rubens M. Nascimento, and José G.A. Pacheco. Characterization and Acidic Properties of AlMCM-41 Prepared by Conventional and Post-Synthesis Alumination. *Australian Journal of Chemistry*, 68(1):99–105, 6 2014.

(7) Erik Krogh Andersen, Inger G. Krogh Andersen, and Gudrun Ploug-Sørensen. Disorder in natrolites: structure determinations of three disordered natrolites and one lithium-exchanged disordered natrolite. *European Journal of Mineralogy*, 2(6):799–808, 12 1990.

(8) Qing Zhang, Yi Zhai, Fumin Wang, Xubin Zhang, Guojun Lv, Yongkui Liu, Mengyue Li, and Mengyao Li. One-step controllable strategy for synthesizing hierarchical Fe-MFI/MCM-41 composites using CTAB as a dual-functional template. *Microporous and Mesoporous Materials*, 329(October 2021):111515, 2022.

(9) P. W.J.G. Wijnen, T. P.M. Beelen, J. W. de Haan, C. P.J. Rummens, L. J.M. van de Ven, and R. A. van Santen. Silica gel dissolution in aqueous alkali metal hydroxides studied by 29SiNMR. *Journal of Non-Crystalline Solids*, 109(1):85–94, 5 1989.

(10) P. W.J.G. Wijnen, T. P.M. Beelen, J. W. De Haan, L. J.M. Van De Ven, and R. A. Van Santen. The structure directing effect of cations in aqueous silicate solutions. A 29Si-NMR study. *Colloids and Surfaces*, 45(C):255–268, 1 1990.

(11) Lingqian Meng, Brahim Mezari, Maarten G. Goesten, and Emiel J.M. Hensen. One-Step Synthesis of Hierarchical ZSM-5 Using Cetyltrimethylammonium as Mesoporogen and Structure-Directing Agent. *Chemistry of Materials*, 29(9):4091–4096, 5 2017.